NANO LETTERS

pubs.acs.org/NanoLett Letter

Tip-Induced In-Plane Ferroelectric Superstructure in Zigzag-Wrinkled $BaTiO_3$ Thin Films

Yuqing Zhou,[⊥] Changqing Guo,[⊥] Guohua Dong,[⊥] Haixia Liu, Ziyao Zhou, Ben Niu, Di Wu, Tao Li,* Houbing Huang,* Ming Liu,* and Tai Min

Cite This: *Nano Lett.* 2022, 22, 2859−2866 Read Online

ACCESS | Metrics & More | Article Recommendations | Supporting Information

ABSTRACT: The complex micro-/nanoscale wrinkle morphology primarily fabricated by elastic polymers is usually designed to realize unique functionalities in physiological, biochemical, bioelectric, and optoelectronic systems. In this work, we fabricated inorganic freestanding $BaTiO_3$ ferroelectric thin films with zigzag wrinkle morphology and successfully modulated the ferroelectric domains to form an in-plane (IP) superstructure with periodic surface charge distribution. Our piezoresponse force microscopy (PFM) measurements and phase-field simulation demonstrate that the self-organized strain/stress field in the zigzag-wrinkled $BaTiO_3$ film generates a corresponding pristine domain structure. These domains can be switched by tip-induced strain gradient (flexoelectricity) and naturally form a robust and unique "braided" in-plane domain pattern, which enables us to offer an effective and convenient way to create a microscopic ferroelectric superstructure. The corresponding periodic surface potential distribution provides an extra degree of freedom in addition to the morphology that could regulate cells or polar molecules in physiological and bioelectric applications.

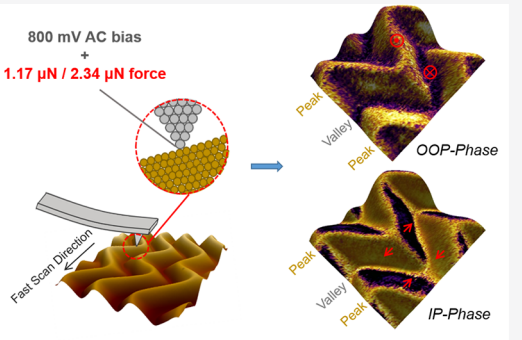

KEYWORDS: *zigzag wrinkle, ferroelectrics, domain engineering, piezoelectricity, flexoelectricity*

INTRODUCTION

Wrinkled morphology is ubiquitous in biological systems, such as white blood cells, papillae on a rose petal, bronchioles, fingerprints, mucosa, and brain cortex in a growing length scale.[1] The dynamic wrinkled morphology has the function of regulating the physiological, biochemical, and physical properties of biological systems. Inspired by mother nature, many biomimetic wrinkled structures have been fabricated for the purposes of self-cleaning,[2] humidity and pressure sensing,[3,4] cell culture,[5,6] tuning hydrophobicity,[7,8] and marine antifouling.[9,10] These functional wrinkled structures are made from flexible polymers or two-dimensional materials, and the functionalities are mainly originated from the specially designed morphology and strain field.[11−14] Recently, the successful fabrication of superelastic and parallel-wrinkled inorganic ferroelectric perovskites has been realized.[15,16] This evokes the possibility to investigate functional wrinkled surfaces based on stiff inorganic materials. Particularly, in addition to the patterned topography, the corresponding electrically charged surface of ferroelectric materials can provide an additional degree of freedom to modulate the electric-field-sensitive matters, such as cells, bacteria, polar molecules, and so on. $BaTiO_3$ (BTO) is a biocompatible classic ferroelectric material. BTO nanoparticles have been employed as nanocarriers for drug delivery.[17] We use BTO films as a representative sample to demonstrate the zigzag-wrinkled morphology induced remarkable ferroelectric behaviors, such as the ferroelectric domain pattern shaped by the complex zigzag-wrinkled structure and the modulation of the ferroelectric domain orientation on top of the zigzag morphology.

In this work, we successfully fabricated three-dimensional freestanding periodic zigzag-wrinkled BTO ferroelectric thin films. Different from the interfacial stress/strain due to the lattice mismatch with the substrate in conventional epitaxial films, the film here possesses unique internal periodic stress/strain distribution. Our phase-field simulation verified that the zigzag morphology leads to a complex strain and domain distribution, which can be modulated by a tip-induced loading force. The morphology-induced self-organized strain field shapes the pristine domain into a metastable state that can be easily switched to a robust "braided" in-plane (IP) domain superstructure and opposite out-of-plane (OOP) domains between peaks and valleys by tip-induced local strain gradient (flexoelectricity effect). The braid-shaped IP ferroelectric

Received: January 5, 2022
Revised: March 11, 2022
Published: March 21, 2022

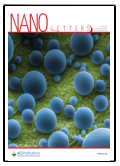

https://doi.org/10.1021/acs.nanolett.1c05028
Nano Lett. 2022, 22, 2859−2866

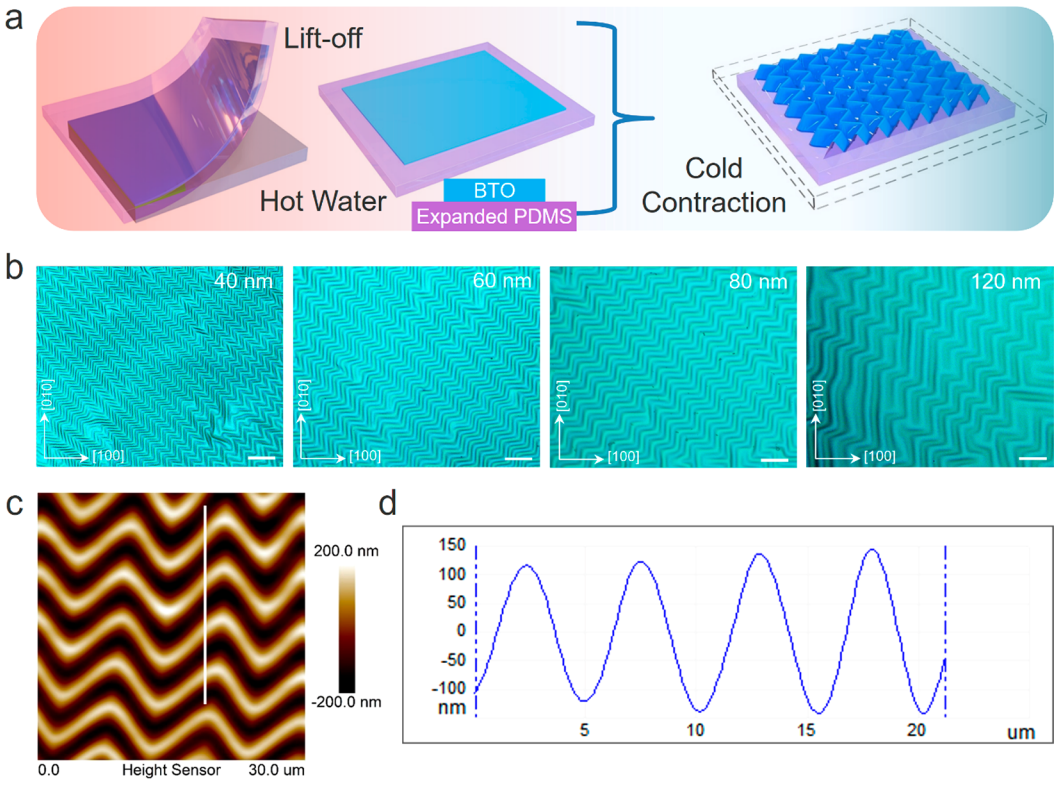

Figure 1. Fabrication of zigzag-wrinkled BTO film. (a) Schematic of zigzag-wrinkled BTO film fabrication. (b) Optical images of zigzag-wrinkled BTO film with different thicknesses. Scale bars are 20 μm. (c) AFM image of zigzag-wrinkled BTO film with thickness of 40 nm. (d) Profile of the corresponding height data along the white line in (c).

superstructure has never been observed in epitaxial ferroelectric thin films. Here, we offer an effective and convenient way to create robust intricate ferroelectric superstructures, which is more efficient than some conventional approaches, such as periodic electrodes and epitaxial strains.[18−20] In addition to the functional morphology, the unique periodic surface potential associated with wrinkled ferroelectric film can help effectively tune cell functions, light field, or polar molecules in the fields of bioelectric control, electro-optic devices, and electrostatic modulation, respectively.

RESULTS AND DISCUSSION

Wrinkling of a stiff film can be realized by transferring it onto a soft elastomeric substrate, which forms a bilayer system. A large mechanical strain mismatch between the two layers can be induced during a cooling process. We have successfully fabricated the zigzag-wrinkled BTO in the bilayer system of a single crystal BTO on a Polydimethylsiloxane (PDMS) substrate (Figure 1). The X-ray diffraction (XRD) result indicates that a single crystal (001) BTO film was obtained by pulsed laser deposition (PLD) method, as shown in Figure S2. First, the PDMS/$BaTiO_3$/$Sr_3Al_2O_6$/$SrTiO_3$ (PDMS/BTO/SAO/STO) heterostructure was immersed in hot water and reached thermal equilibrium. The sacrificial SAO layer was etched away by water so that PDMS-bonded BTO film was lifted off from STO substrate. When gradually cooling to room temperature, the PDMS layer shows obvious volume shrinkage. BTO has an order of smaller thermal expansion coefficient than PDMS. Thus, the zigzag-wrinkled morphology of the BTO film is formed under biaxial compressive stress during the contraction of PDMS (Figure 1a). Details of the method can be found in the Experimental Details in the Supporting Information and our previous work.[15] The thickness of BTO film has a dramatic influence on the period of wrinkled pattern, as shown in Figure 1b. The thicker the BTO film, the larger the wavelength, which is due to the largely increased buckling strength. The crystallographic directions of BTO membranes along the ⟨100⟩ view are labeled in Figure 1b. Figure 1c shows the AFM image of a typical zigzag-wrinkled BTO film. The wrinkle peak-to-peak amplitude is about 280 nm, and the wavelength is about 5 μm according to the height profile in Figure 1d.

Characterization of the domain structures and polarization switching dynamics can be challenging for the complex wrinkled ferroelectric film because of the highly uneven morphology. In this case, piezoresponse force microscopy (PFM) is the most appropriate method to investigate domain structure. In PFM measurements, the phase images indicate the relative polarization orientation. A 180° phase shift means opposite polarization orientation, whereas the amplitude images reveal the strength of electromechanical response, primarily piezoresponse for ferroelectric materials. We carried out vertical and lateral PFM (VPFM and LPFM) measurements to acquire the OOP (z-axis) and IP (x-axis) ferroelectric responses, respectively. The domain structures are intricate due to the lower symmetry of zigzag morphology and varied strain distribution. After being scanned with a loading force of 2.34 μN, the polarization orientation is switched from a relatively disordered nanodomain state to a "stripe" OOP domain structure with opposite polarization orientations between peak and valley regions and a novel "braided" IP domain structure (Figure 2a). We qualitatively defined the polarization orientation along z- and x-axis after scanning with 2.34 μN loading force, indicated by the gray markers in the

https://doi.org/10.1021/acs.nanolett.1c05028
Nano Lett. 2022, 22, 2859−2866

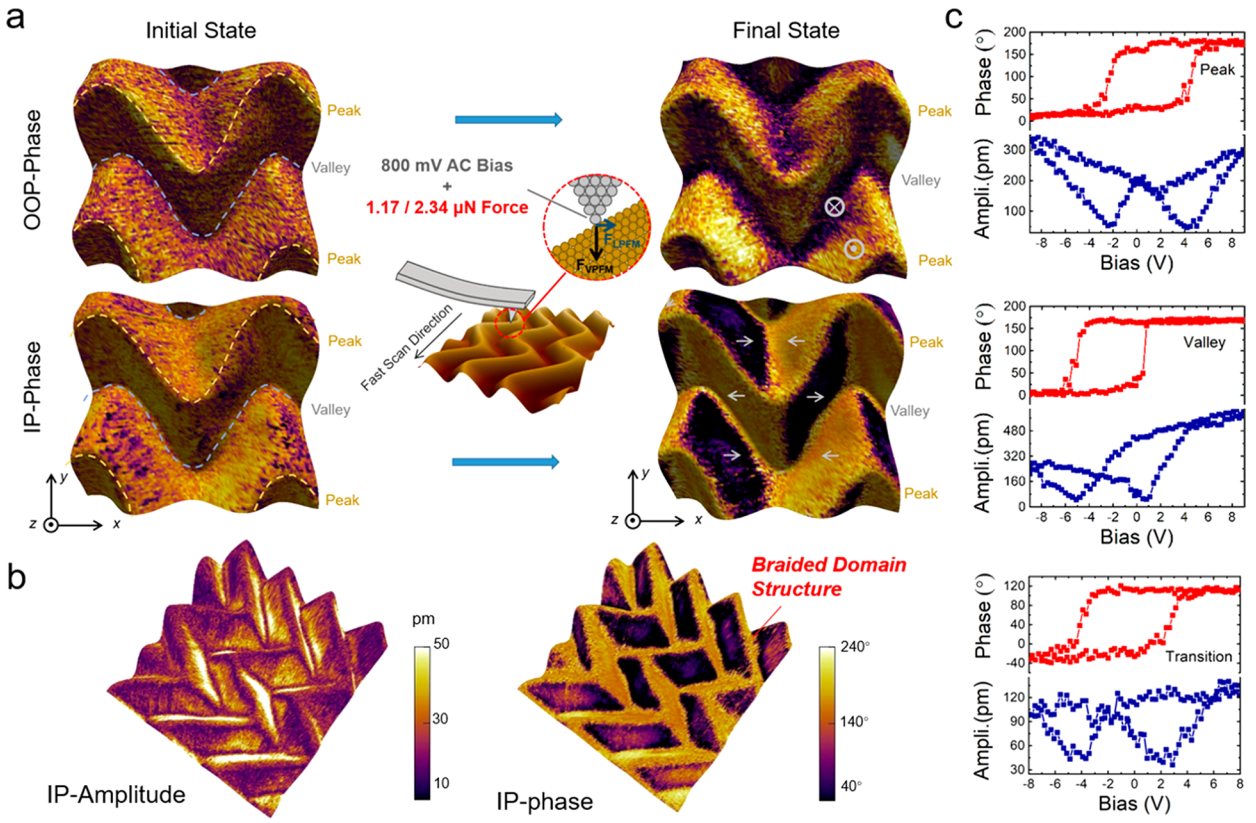

Figure 2. IP and OOP ferroelectric domains of zigzag-wrinkled BTO obtained under large scanning force. (a) PFM phase color images mapped on top of the 3D morphology and the schematic of the domain switching induced by the scanning force of tip. The yellow and gray dotted curves in initial state images indicate the position of peak and valley, respectively; the gray markers in final state (OOP-Phase) image represent the net polarization orientation, and the arrows in final state (IP-Phase) image are qualitative expressions of polarization component along *x*-axis. (b) Typical IP-amplitude and IP-phase images overlapped on 3D morphology after scanning with a 2.34 μN loading force. (c) Typical phase and amplitude hysteresis loops observed at peak, valley, and transition regions, respectively.

Table 1. Statistical Analysis of Characteristics of PFM Hysteresis Loops in the Peak, Valley, and Transition Regions

		imprint/V[b]		effective coercive bias/V[b]		
region	PFM response[a]	mean	sigma	mean	sigma	percentage/%[c]
peak	asym +	−0.83	0.7129	2.425	0.8546	16.67
	asym −	1.29	0.5520	2.99	0.8431	58.33
	sym	0.22	0.6241	2.89	0.8403	25.00
valley	asym +	−1.02	0.5466	3.11	1.1887	47.22
	asym −	0.87	0.6764	2.73	0.5780	33.33
	sym	−0.16	0.4541	3.16	1.3563	19.44
transition	asym +	−1.16	0.4761	3.88	0.8718	40.91
	asym −	1.22	0.5497	4.05	1.3965	27.27
	sym	−0.33	0.6626	3.90	1.0893	31.82

[a]"Asym +" indicates a stronger piezoresponse under positive electric bias; "Asym −" indicates a stronger piezoresponse under negative electric bias. "Sym" indicates a symmetric piezoresponse between negative and positive electric bias. [b]Imprint = $(V_{c+} + V_{c-})/2$. Effective coercive bias = $(V_{c+} - V_{c-})/2$; V_{c+} and V_{c-} are the positive and negative coercive biases, respectively. [c]"Percentage" indicates the probability of the particular type of PFM hysteresis loops appearing in the peak, valley, and transition regions. The loading force during hysteresis loop measurements is 0.73 μN.

final state as shown in Figure 2a. A wider range of domain structures are shown in Figure 2b, which unambiguously exhibits the domain wall between the opposite domain structure (IP-amplitude) and a periodic "braided" ferroelectric superstructure (IP-phase). The scanning force dependent domain evolution process is demonstrated in more detail in section 4 of the Supporting Information. It should be noted that the flexoelectricity field induced by the moderate scanning force (1.17 μN) is not sufficient to overcome the potential barrier and reach a stable state because of the film internal strain. Therefore, the domain structure is relaxed when the scanning force is removed. Besides, we conducted the same PFM measurements on a nonwrinkled freestanding BTO film (Figure S4). It is verified that the tip-induced ferroelectric superstructure is unique to the zigzag-wrinkled BTO film.

The representative amplitude and phase hysteresis loops of peak, valley, and transition regions are shown in Figure 2c. The phase loops clearly demonstrate the polarization switching at all different regions. To understand the effects of global strain/stress field in the zigzag-wrinkled BTO film, around 30

https://doi.org/10.1021/acs.nanolett.1c05028
Nano Lett. 2022, 22, 2859−2866

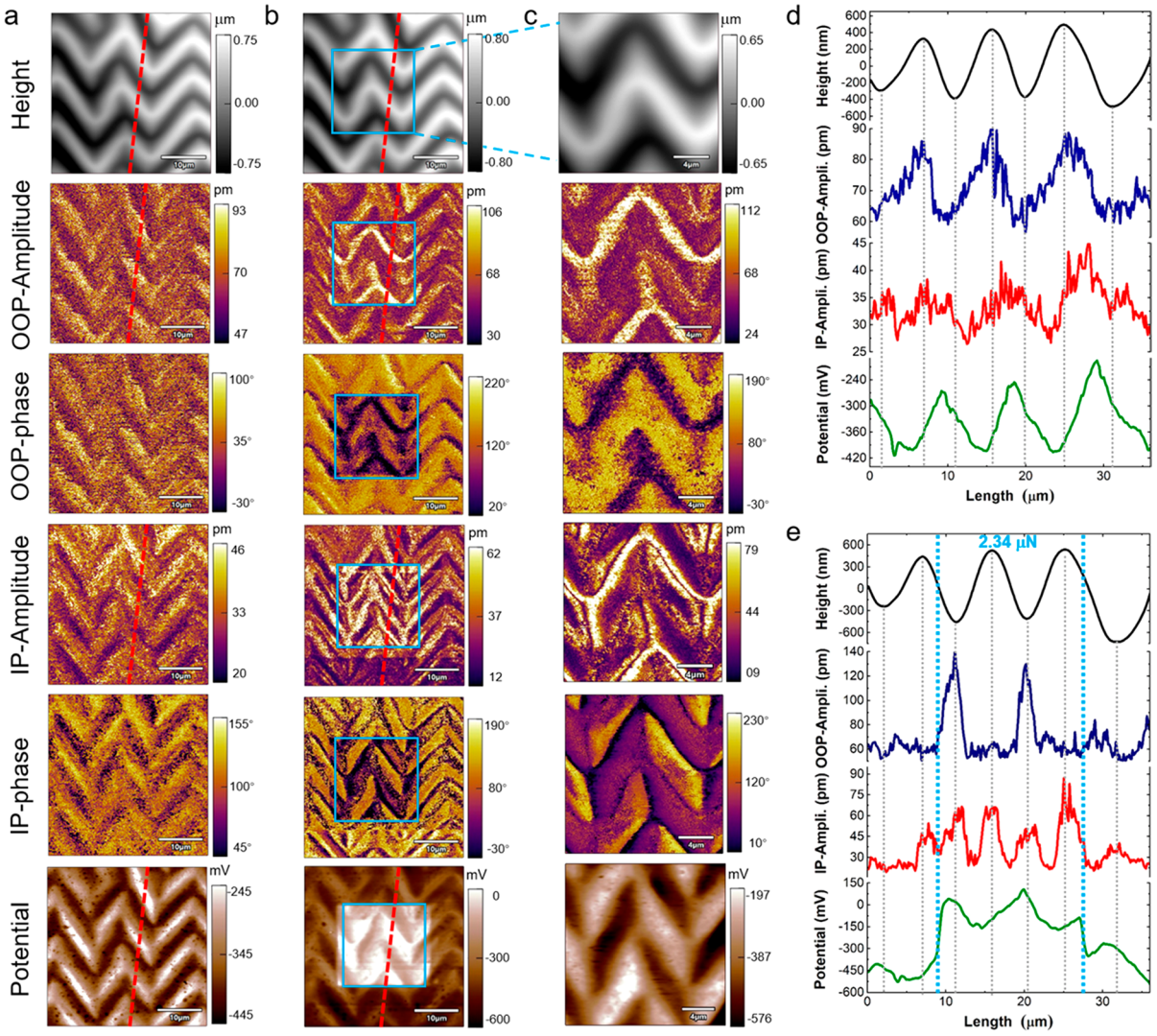

Figure 3. SPM tip-induced flexoelectric effect leads to the domain switching of zigzag-wrinkled BTO film. (a) Pristine VPFM, LPFM, and KPFM images of wrinkled BTO under small loading force (0.26 μN). (b) VPFM, LPFM, and KPFM images of the wrinkled BTO film obtained 12 hours later after the 2.34 μN loading force was applied within the blue square. (c) Zoomed-in VPFM, LPFM, and KPFM images enclosed by the blue square in (b). Scan size is 36 μm × 36 μm for (a) and (b), and 18 μm × 18 μm for (c). (d, e) Line profiles of the corresponding height, OOP-amplitude, IP-amplitude, and potential data (average over 10 pixels) along the red dotted lines in (a) and (b), respectively, where the blue dotted lines in (e) mark the boundary of the part scanned by 2.34 μN loading force before.

hysteresis loops were measured at random locations of peak, valley, and transition regions, respectively. We carried out statistical analysis of these loops to gain an insight into the domain switching dynamics (Table 1). Most of the hysteresis loops in the peak regions have a positive imprint with stronger piezoresponse under negative bias (P_{up} is preferred), and most hysteresis loops in valley regions show a negative imprint with stronger piezoresponse under positive bias (P_{down} is preferred). The effective coercive bias at strained regions (both tensile and compressive) is around 3 V, while at nearly strain-free regions is around 4 V. We also observed that the zigzag-wrinkled BTO film exhibits rich nanodomain structures, which demonstrates that the microscale polarization orientation and strength are the collective polarization states of these nanodomains (Figure S5). The different strain-mediated build-in electric fields inside the nanodomains may explain the variability of hysteresis loop characteristics on the compressive or tensile strain regions, and the details are elaborated in section 7 of the Supporting Information. We have also conducted loading-force-dependent local ferroelectric hysteresis measurements (section 8 of the Supporting Information). With a larger loading force, an increased negative imprint and stronger piezoresponse under positive bias are observed. It indicates that the strain (gradient) induced by the SPM tip can generate an effective build-in field, which facilitates the polarization switching from the P_{up} state to the P_{down} state.

Furthermore, we evaluated the retention of the mechanically induced domain switching by a SPM tip on the zigzag-wrinkled BTO film. In Figure 3b, the central area enclosed by a blue square was scanned with 2.34 μN loading force, and the whole area was then scanned again with a small loading force (0.26 μN) 12 hours later. Stable OOP and IP ferroelectric domains are created when the scanning force is sufficiently large (2.34 μN). In the case of flat epitaxial ferroelectric thin films, ferroelectric domains are generally switched to the OOP downward polarization by flexoelectricity.[21,22] One exception is that by adjusting the motion of an SPM tip,[23] the very localized IP polarization switching is observed in particular

https://doi.org/10.1021/acs.nanolett.1c05028
Nano Lett. 2022, 22, 2859−2866

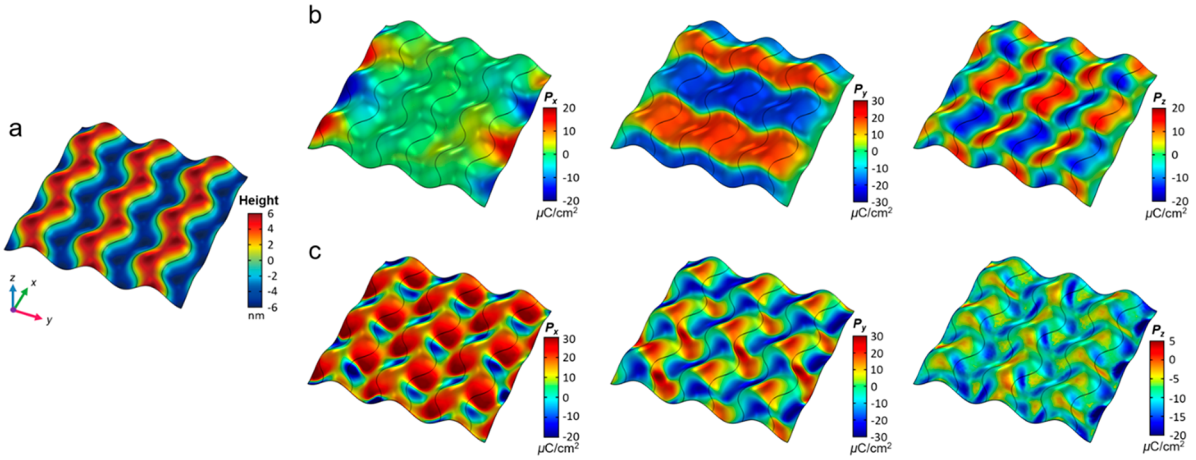

Figure 4. Phase-field simulation of the domain structure of zigzag-wrinkled BTO modulated by the scanning force induced by an SPM tip. The model size is 120 nm × 120 nm. (a) Height distribution of zigzag-wrinkled BTO. (b) Distribution of IP polarization component P_x (along x-axis), P_y (along the y-axis), and OOP polarization component P_z (along the z-axis) of pristine zigzag-wrinkled BTO. (c) Distribution IP polarization components P_x and P_y under 1% external OOP strain scanning along the x-axis, and OOP polarization component P_z under 5% external OOP strain scanning along the x-axis.

orientations of a $BiFeO_3$ film. In our work, the periodic wrinkled ferroelectric film endows flexoelectric effect an ability to switch both OOP and IP polarizations regardless of the tip motion. Instead of the highly localized IP domains, we demonstrate a convenient way to generate a robust IP ferroelectric superstructure. The zoomed-in VPFM and LPFM images of this permanently switched region are shown in Figure 3c. The domain structure is due to the morphology-induced internal stress/strain distribution and the robust flexoelectric effect induced by the SPM tip. Comparing the PFM-phase images in Figure 3a,b, the valley region is switched to P_{down}, and some IP domains are also switched to the opposite directions and formed a periodically arranged "braided" domain structure with clear head-to-head and tail-to-tail domain walls. The line profiles of the height, OOP-amplitude, IP-amplitude, and surface potential images in Figure 3a,b are shown in Figure 3d,e, respectively. The line-profiles unambiguously exhibit the strongest OOP piezoresponse shifts from the peak region to the valley region, and the IP piezoresponse and surface potential of the entire blue square are enhanced. In our former research on parallel-wrinkled BTO,[15] the compressive stress/strain dominated valley surface possesses a greater OOP component of effective polarization, while the tensile strain dominated peak surface possesses a greater IP component of effective polarization. In the case of the zigzag wrinkled BTO, the valley regions also exhibit a much stronger OOP response than that of peak regions after the tip-induced domain switching. The IP piezoresponse and domain structure are due to the interplay between the morphology-induced internal stress/strain distribution and the robust flexoelectric effect induced by the SPM tip. Kelvin probe force microscope (KPFM) results before and after the tip-induced domain switching indicate that the surface potential can be tailored by the corresponding ferroelectric domain structure (Figures 3 and S8). Many reported data[24−26] show that ferroelectric materials in the P_{down} orientation have higher surface potential compared with that of the P_{up} orientation. In the pristine state, surface potential is strongly correlated with the film morphology (Figure 3a). The zigzag peak region generally has a lower potential than that of the valley region. After applying a strong loading force, the surface potential of the film is substantially increased, which is in consistent with the flexoelectric effect induced polarization switching towards the P_{down} orientation. When we investigated the switched region in detail, the relation between surface potential and morphology is broken. Now it is closely correlated to the newly evolved IP domain structure (Figure 3c). Such a versatile surface potential tuned by the ferroelectric domains in zigzag-wrinkled BTO films provides a promising alternative in flexible nanoscale electronic, micromechanical, and biomedical applications.

To discern the 3D domain structure of the wrinkled BTO film, we also conducted VPFM (OOP), x-LPFM (IP parallel to wrinkle axis), and y-LPFM (IP normal to wrinkle axis) of the same region with 1.44 μN scanning force (Figure S9). We found that the VPFM response is stronger in the valley regions and results in a "striped" domain structure corresponding to the morphology. The y-LPFM response shows a multidomain structure at peak region, whereas a rather uniform domain at valley regions. On the basis of the piezoresponse and domain structure observed at different orientations, the IP domain should be preferably along the wrinkle axis.

We conducted phase-field simulations to gain a deeper understanding of the ferroelectric domain switching induced by the superimposed strain/stress from the zigzag-wrinkled morphology and SPM tip, and the detailed simulation method is shown in section 2 of the Supporting Information. Figure 4 shows the morphology, IP polarization components P_x (along x-axis) and P_y (along y-axis), and OOP polarization component P_z of zigzag-wrinkled BTO at pristine state and under a loading force. The black curved lines indicate the boundaries between peak and valley regions. As shown in Figure 4b, the pristine polarizations are relatively disordered and weak along x-axis. Along y-axis, strong polarizations form a "striped" domain structure perpendicular to the wrinkle-propagating direction. Along the z-axis, the relatively large polarizations exhibit a periodic distribution at the side wall of the wrinkled structure. However, we did not obtain similar experimental results in the pristine state, which is probably due to a more complicated stress/strain distribution in a real sample and therefore generates a disordered domain state with small effective polarization. Under the scanning force applied

https://doi.org/10.1021/acs.nanolett.1c05028
Nano Lett. 2022, 22, 2859−2866

by a SPM tip, a strong polarization component is along the *x*-axis and a novel braided domain structure is observed in both the peak and valley regions of the zigzag-wrinkled BTO film (P_x in Figure 4c). The polarization along the *y*-axis has a different kind of periodic domain structure. The OOP domains are switched to the conditions of more P_{up} domains in the peak regions and much stronger P_{down} domains in the valley regions (P_z in Figure 4c). The simulation results of the stressed state are in consistent with our PFM measurements. The corresponding polarization vectors mapped on the 3D morphology are shown in Figure S10. The resultant domain switching behavior should be modulated by the unique coupled strain conditions induced by the wrinkled morphology and the SPM tip. In general, the normal strain components can directly switch the polarization orientation by 180°, and the shear strain components will induce an in-plane shift of polarization orientation.[27] Therefore, we further simulated the strain distribution at the pristine state and stressed state under scanning force (Figure S11). It is evident that the loading force applied by the SPM tip (local external strain) interacts with the internal strain of zigzag-wrinkled morphology and triggers a striking change of strain conditions. It results in the IP braided domain superstructure and the opposite OOP polarizations between the peak and valley regions. The observed novel braided IP domain structures along the *x*-axis are the result of a strong coupling effect between the normal strain component ε_{xx} and shear strain components ε_{xy} and ε_{xz}. To clarify the effect of flexoelectricity on the tip-induced domain switching process, we also simulate the polarization components with and without flexoelectricity. When flexoelectricity has been considered, the results are in more consistent with the PFM results (Figure S12). We further simulated the flexoelectric effect induced by the wrinkle morphology and by the SPM tip, respectively, as shown in Figure S13. The results verify our conclusion that flexoelectric effect induced by SPM tip dominates the stable mechanical-induced domain switching.

CONCLUSION

In this work, we fabricated 3D freestanding periodic zigzag-wrinkled inorganic BTO ferroelectric thin films and investigated the pristine domain structure and the intricate domain evolution induced by the tip-loading force. The PFM results manifest a pristine microscopic domain structure closely correlated with the zigzag morphology. Massive nanoscale domains exist in these microscale domain features, which can be modulated by varied scanning force applied by the SPM tip. Under a relatively large loading force, we consistently observed opposite OOP polarization orientation between peak and valley regions and a novel "braided" shape of IP domain superstructure. The resultant behavior of the wrinkled film can be interpreted as the coupling between the internal strain/stress field of the zigzag-wrinkled morphology and the flexoelectric effect induced by the SPM tip. Different from other works, the flexoelectricity here can switch both OOP and IP polarization orientation. The phase-field simulation results unambiguously manifest the domain switching behaviors of the zigzag-wrinkled ferroelectric thin film caused by the tip-induced flexoelectricity. Such flexible ferroelectric thin films with zigzag morphology and tunable ferroelectricity, as well as the corresponding periodic electric potential distribution according to the KPFM results, can be used in flexible sensors, bioelectric control, electro-optic devices, electrostatic modulation, and other related fields.

ASSOCIATED CONTENT

Supporting Information

The Supporting Information is available free of charge at https://pubs.acs.org/doi/10.1021/acs.nanolett.1c05028.

Experimental details; phase-field simulation method; X-ray diffraction characterization of the $BaTiO_3/Sr_3Al_2O_6/SrTiO_3$ sample; domain switching process modulated by the loading force; tip-induced domain switching on nonwrinkled freestanding BTO film; nanodomain structure of the wrinkled BTO; local domain switching dynamics of the wrinkled BTO; ferroelectric hysteresis affected by the loading force; pristine surface potential distribution of the wrinkled BTO; domain structures along the *x*, *y*, and *z* orientations; phase-field simulated 3D polarization distribution; phase-field simulated strain distribution; phase-field simulated flexoelectric effect (PDF)

AUTHOR INFORMATION

Corresponding Authors

Tao Li − *Center for Spintronics and Quantum Systems, State Key Laboratory for Mechanical Behavior of Materials, Department of Materials Science and Engineering, Xi'an Jiaotong University, Xi'an 710049, China*; Email: taoli66@xjtu.edu.cn

Houbing Huang − *School of Materials Science and Engineering & Advanced Research Institute of Multidisciplinary Science, Beijing Institute of Technology, Beijing 100081, China*; orcid.org/0000-0002-8006-3495; Email: hbhuang@bit.edu.cn

Ming Liu − *The Electronic Materials Research Laboratory, Key Laboratory of the Ministry of Education & International Center for Dielectric Research, School of Electronic Science and Engineering, State Key Laboratory for Mechanical Behavior of Materials, Xi'an Jiaotong University, Xi'an 710049, China*; orcid.org/0000-0002-6310-948X; Email: mingliu@xjtu.edu.cn

Authors

Yuqing Zhou − *Center for Spintronics and Quantum Systems, State Key Laboratory for Mechanical Behavior of Materials, Department of Materials Science and Engineering, Xi'an Jiaotong University, Xi'an 710049, China*; orcid.org/0000-0001-7986-5338

Changqing Guo − *School of Materials Science and Engineering & Advanced Research Institute of Multidisciplinary Science, Beijing Institute of Technology, Beijing 100081, China*

Guohua Dong − *The Electronic Materials Research Laboratory, Key Laboratory of the Ministry of Education & International Center for Dielectric Research, School of Electronic Science and Engineering, State Key Laboratory for Mechanical Behavior of Materials, Xi'an Jiaotong University, Xi'an 710049, China*

Haixia Liu − *The Electronic Materials Research Laboratory, Key Laboratory of the Ministry of Education & International Center for Dielectric Research, School of Electronic Science and Engineering, State Key Laboratory for Mechanical Behavior of Materials, Xi'an Jiaotong University, Xi'an 710049, China*

Ziyao Zhou − *The Electronic Materials Research Laboratory, Key Laboratory of the Ministry of Education & International*

https://doi.org/10.1021/acs.nanolett.1c05028
Nano Lett. 2022, 22, 2859−2866

Center for Dielectric Research, School of Electronic Science and Engineering, State Key Laboratory for Mechanical Behavior of Materials, Xi'an Jiaotong University, Xi'an 710049, China; orcid.org/0000-0002-5484-5442

Ben Niu − *National Laboratory of Solid State Microstructures, Department of Materials Science and Engineering, Jiangsu Key Laboratory for Artificial Functional Materials, Nanjing University, Nanjing 210093, China*

Di Wu − *National Laboratory of Solid State Microstructures, Department of Materials Science and Engineering, Jiangsu Key Laboratory for Artificial Functional Materials, Nanjing University, Nanjing 210093, China;* orcid.org/0000-0003-3619-1411

Tai Min − *Center for Spintronics and Quantum Systems, State Key Laboratory for Mechanical Behavior of Materials, Department of Materials Science and Engineering, Xi'an Jiaotong University, Xi'an 710049, China*

Complete contact information is available at: https://pubs.acs.org/10.1021/acs.nanolett.1c05028

Author Contributions

⊥Y.Z., C.G., and G.D. contributed equally to this work.

Notes

The authors declare no competing financial interest.

■ ACKNOWLEDGMENTS

This work was financially supported by the National Key R&D Program of China (Grant No. 2021YFA1202200, 2017YFA0206202, 2018YFB0407601, 2019YFA0307900), the National Natural Science Foundation of China (Grant No. 51802250, 51972028, 91964109, 52002310), and the Key R&D Program of Shaanxi (Program No. 2019TSLGY08).

■ REFERENCES

(1) Tan, Y.; Hu, B.; Song, J.; Chu, Z.; Wu, W. Bioinspired Multiscale Wrinkling Patterns on Curved Substrates: An Overview. *Nano-Micro Lett.* **2020**, *12* (1), 101.

(2) Pocivavsek, L.; Ye, S.-H.; Pugar, J.; Tzeng, E.; Cerda, E.; Velankar, S.; Wagner, W. R. Active Wrinkles to Drive Self-Cleaning: A Strategy for Anti-Thrombotic Surfaces for Vascular Grafts. *Biomaterials* **2019**, *192*, 226−234.

(3) Miao, L.; Wan, J.; Song, Y.; Guo, H.; Chen, H.; Cheng, X.; Zhang, H. Skin-Inspired Humidity and Pressure Sensor with a Wrinkle-on-Sponge Structure. *ACS Appl. Mater. Interfaces* **2019**, *11* (42), 39219−39227.

(4) Baek, S.; Jang, H.; Kim, S. Y.; Jeong, H.; Han, S.; Jang, Y.; Kim, D. H.; Lee, H. S. Flexible Piezocapacitive Sensors Based on Wrinkled Microstructures: Toward Low-Cost Fabrication of Pressure Sensors over Large Areas. *RSC Adv.* **2017**, *7* (63), 39420−39426.

(5) Izawa, H.; Okuda, N.; Yonemura, T.; Kuroda, K.; Ochi, K.; Ifuku, S.; Morimoto, M.; Saimoto, H.; Noda, M.; Azuma, K.; Okamoto, Y.; Ito, N. Application of Bio-Based Wrinkled Surfaces as Cell Culture Scaffolds. *Colloid Interface* **2018**, *2* (2), 15.

(6) Nguyen, D. H. K.; Bazaka, O.; Bazaka, K.; Crawford, R. J.; Ivanova, E. P. Three-Dimensional Hierarchical Wrinkles on Polymer Films: From Chaotic to Ordered Antimicrobial Topographies. *Trends Biotechnol* **2020**, *38* (5), 558−571.

(7) Wang, D.; Xu, L.; Zhang, L.; Zhang, L.; Zhang, A. Hydrophobic/Superhydrophobic Reversible Smart Materials Via Photo/Thermo Dual-Response Dynamic Wrinkled Structure. *Chemical Engineering Journal* **2021**, *420*, 127679.

(8) Sahoo, B. N.; Woo, J.; Algadi, H.; Lee, J.; Lee, T. Superhydrophobic, Transparent, and Stretchable 3d Hierarchical Wrinkled Film-Based Sensors for Wearable Applications. *Adv. Mater. Technol.* **2019**, *4* (10), 1900230.

(9) Ware, C. S.; Smith-Palmer, T.; Peppou-Chapman, S.; Scarratt, L. R. J.; Humphries, E. M.; Balzer, D.; Neto, C. Marine Antifouling Behavior of Lubricant-Infused Nanowrinkled Polymeric Surfaces. *ACS Appl. Mater. Interfaces* **2018**, *10* (4), 4173−4182.

(10) Owais, A.; Smith-Palmer, T.; Gentle, A.; Neto, C. Influence of Long-Range Forces and Capillarity on the Function of Underwater Superoleophobic Wrinkled Surfaces. *Soft Matter* **2018**, *14* (32), 6627−6634.

(11) Hou, H.; Yin, J.; Jiang, X. Smart Patterned Surface with Dynamic Wrinkles. *Acc. Chem. Res.* **2019**, *52* (4), 1025−1035.

(12) Li, F.; Hou, H.; Yin, J.; Jiang, X. Near-Infrared Light−Responsive Dynamic Wrinkle Patterns. *Sci. Adv.* **2018**, *4* (4), No. eaar5762.

(13) Li, Y.; Tian, X.; Gao, S.-P.; Jing, L.; Li, K.; Yang, H.; Fu, F.; Lee, J. Y.; Guo, Y.-X.; Ho, J. S.; Chen, P.-Y. Reversible Crumpling of 2d Titanium Carbide (Mxene) Nanocoatings for Stretchable Electromagnetic Shielding and Wearable Wireless Communication. *Adv. Funct. Mater.* **2020**, *30* (5), 1907451.

(14) Zhang, X. A.; Jiang, Y.; Venkatesh, R. B.; Raney, J. R.; Stebe, K. J.; Yang, S.; Lee, D. Scalable Manufacturing of Bending-Induced Surface Wrinkles. *ACS Appl. Mater. Interfaces* **2020**, *12* (6), 7658−7664.

(15) Dong, G.; Li, S.; Li, T.; Wu, H.; Nan, T.; Wang, X.; Liu, H.; Cheng, Y.; Zhou, Y.; Qu, W.; Zhao, Y.; Peng, B.; Wang, Z.; Hu, Z.; Luo, Z.; Ren, W.; Pennycook, S. J.; Li, J.; Sun, J.; Ye, Z.-G.; Jiang, Z.; Zhou, Z.; Ding, X.; Min, T.; Liu, M. Periodic Wrinkle-Patterned Single-Crystalline Ferroelectric Oxide Membranes with Enhanced Piezoelectricity. *Adv. Mater.* **2020**, *32* (50), 2004477.

(16) Dong, G.; Li, S.; Yao, M.; Zhou, Z.; Zhang, Y.-Q.; Han, X.; Luo, Z.; Yao, J.; Peng, B.; Hu, Z.; Huang, H.; Jia, T.; Li, J.; Ren, W.; Ye, Z.-G.; Ding, X.; Sun, J.; Nan, C.-W.; Chen, L.-Q.; Li, J.; Liu, M. Super-Elastic Ferroelectric Single-Crystal Membrane with Continuous Electric Dipole Rotation. *Science* **2019**, *366* (6464), 475.

(17) Genchi, G. G.; Marino, A.; Rocca, A.; Mattoli, V.; Ciofani, G. Barium Titanate Nanoparticles: Promising Multitasking Vectors in Nanomedicine. *Nanotechnology* **2016**, *27* (23), 232001.

(18) Li, D.; Bonnell, D. A. Controlled Patterning of Ferroelectric Domains: Fundamental Concepts and Applications. *Annu. Rev. Mater. Res.* **2008**, *38* (1), 351−368.

(19) Wada, S. Domain Wall Engineering in Lead-Free Piezoelectric Materials and Their Enhanced Piezoelectricities. In *Next-Generation Actuators Leading Breakthroughs*; Higuchi, T., Suzumori, K., Tadokoro, S., Eds.; Springer: London, 2010; pp 227−243.

(20) Matzen, S.; Nesterov, O.; Rispens, G.; Heuver, J. A.; Biegalski, M.; Christen, H. M.; Noheda, B. Super Switching and Control of in-Plane Ferroelectric Nanodomains in Strained Thin Films. *Nat. Commun.* **2014**, *5* (1), 4415.

(21) Lu, H.; Bark, C.-W.; Esque de los Ojos, D.; Alcala, J.; Eom, C. B.; Catalan, G.; Gruverman, A. Mechanical Writing of Ferroelectric Polarization. *Science* **2012**, *336* (6077), 59−61.

(22) Očenášek, J.; Lu, H.; Bark, C. W.; Eom, C. B.; Alcalá, J.; Catalan, G.; Gruverman, A. Nanomechanics of Flexoelectric Switching. *Phys. Rev. B* **2015**, *92* (3), 035417.

(23) Park, S. M.; Wang, B.; Das, S.; Chae, S. C.; Chung, J.-S.; Yoon, J.-G.; Chen, L.-Q.; Yang, S. M.; Noh, T. W. Selective Control of Multiple Ferroelectric Switching Pathways Using a Trailing Flexoelectric Field. *Nat. Nanotechnol.* **2018**, *13* (5), 366−370.

(24) Kalinin, S. V.; Kim, Y.; Fong, D. D.; Morozovska, A. N. Surface-Screening Mechanisms in Ferroelectric Thin Films and Their Effect on Polarization Dynamics and Domain Structures. *Rep. Prog. Phys.* **2018**, *81* (3), 036502.

(25) Li, T.; Lipatov, A.; Lu, H.; Lee, H.; Lee, J.-W.; Torun, E.; Wirtz, L.; Eom, C.-B.; Iniguez, J.; Sinitskii, A.; Gruverman, A. Optical Control of Polarization in Ferroelectric Heterostructures. *Nat. Commun.* **2018**, *9* (1), 3344.

(26) Collins, L.; Kilpatrick, J. I.; Bhaskaran, M.; Sriram, S.; Weber, S. A. L.; Jarvis, S. P.; Rodriguez, B. J. Dual Harmonic Kelvin Probe Force Microscopy for Surface Potential Measurements of Ferroelectrics. *Proceedings of ISAF-ECAPD-PFM 2012* **2012**, *9*−*13*, 1−4.

(27) Yuan, S.; Chen, W.; Liu, J.; Liu, Y.; Wang, B.; Zheng, Y. Torsion-Induced Vortex Switching and Skyrmion-Like State in Ferroelectric Nanodisks. *J. Phys.: Condens. Matter* **2018**, *30* (46), 465304.

https://doi.org/10.1021/acs.nanolett.1c05028
Nano Lett. 2022, 22, 2859−2866